

Angiography-based radial wall strain in carotid plaques and its association with plaque vulnerability

Shiteng Suo¹, PhD; Huilin Zhao², MD; Chunming Li³, BSc; Mengqiu Cao², MD; Zhiqing Wang⁴, MD; Jin Zhang², MD; Tonglei Han⁵, MD; Daqiao Guo⁵, MD; Weiguo Fu⁵, MD; Yan Zhou², MD; Shengxian Tu^{3*}, PhD

*Corresponding author: Room 123, Med-X Research Institute, Shanghai Jiao Tong University, No. 1954, Hua Shan Road, Xuhui District, Shanghai, 200030, China. E-mail: sxtu@sjtu.edu.cn

This paper also includes supplementary data published online at: <https://eurointervention.pconline.com/doi/10.4244/EIJ-D-24-00734>

For improved risk stratification of carotid stenosis, it is necessary to incorporate factors beyond mere stenosis severity¹. Biomechanics is a key factor contributing to plaque vulnerability². Our study introduces angiography-derived radial wall strain (RWS) to analyse carotid stenosis biomechanics and their association with plaque composition and vulnerability.

We included consecutive patients with internal carotid artery stenosis undergoing both carotid 3.0T magnetic resonance imaging (MRI) and digital subtraction angiography (DSA) within 1 week between July 2019 and December 2021 (**Supplementary Figure 1**). RWS was calculated as the ratio of the difference between the maximum and minimum lumen diameter (i.e., max–min) to the maximum diameter after automatic lumen segmentation and registration of four representative DSA frames of the cardiac cycle³ (**Central illustration**). RWS_{max} represented the lesion's maximum RWS value. Plaque composition and vulnerability were determined by carotid MRI (**Supplementary Table 1, Supplementary Figure 2**). A detailed description of the eligibility criteria, carotid DSA and RWS analysis, carotid MRI and image interpretation, and statistical analysis is provided in **Supplementary Appendix 1**.

After screening, 110 patients (mean age 67.7±7.2 years; 94 males; 79 symptomatic) with 135 plaques were studied (**Supplementary Table 2**). RWS analysis was feasible and reproducible, and the mean analysis time per lesion was 59±30 seconds (**Supplementary Figure 3, Supplementary Appendix 2, Supplementary Figure 4**). The majority of analysed plaques were based on the lateral view (119/135). RWS_{max} showed weak to moderate correlations with morphological features, such as percentage diameter stenosis (DS%) (**Supplementary**

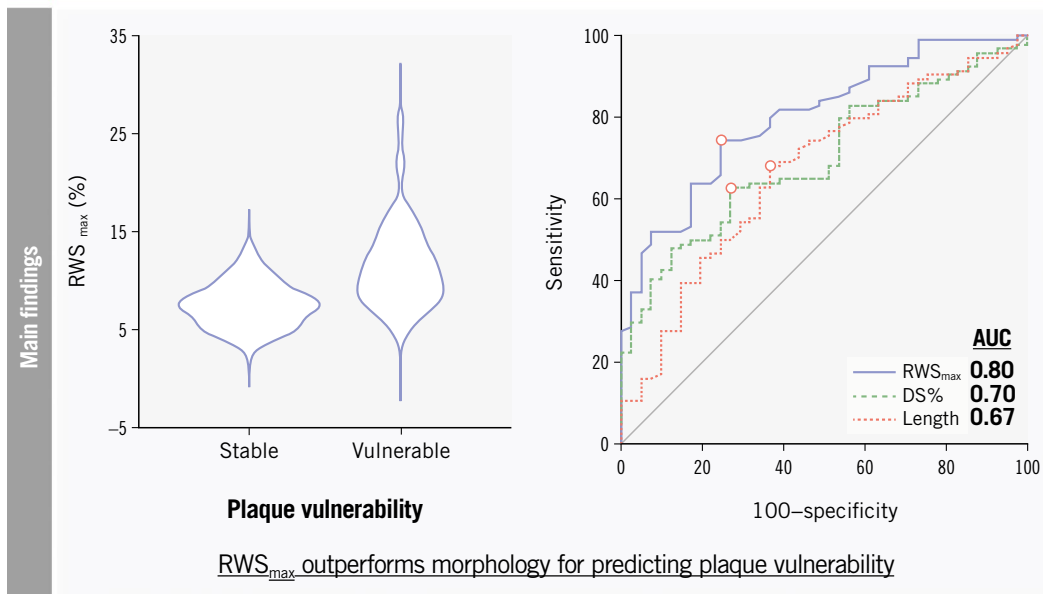
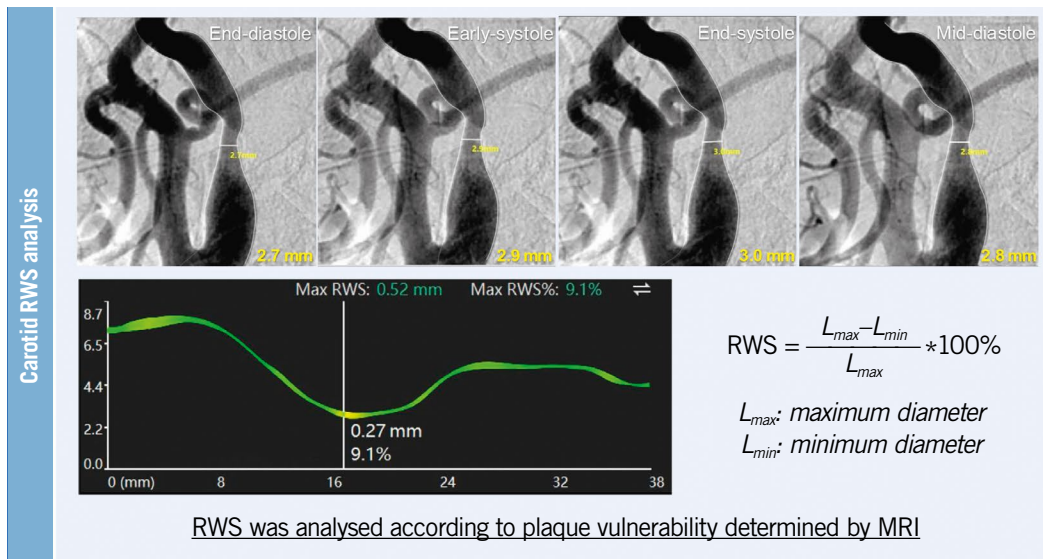
Figure 5). RWS_{max} was higher in plaques containing intraplaque haemorrhage or a large lipid-rich necrotic core, and in those developing fibrous cap rupture (**Supplementary Figure 6**). Overall, the median RWS_{max} value was 11.0% in vulnerable plaques versus 7.5% in stable plaques, with an area under the receiver operating characteristic curve (AUC) of 0.80 for discrimination (**Central illustration**). A cutoff value of 8.5% achieved the maximum Youden index (sensitivity=74.5%; specificity=75.6%) (**Supplementary Table 3**). Representative cases are illustrated in **Supplementary Figure 7**.

Similarly, in plaque subgroups with different degrees of stenosis (<50% and 50–99%) or symptomatic statuses (symptomatic and asymptomatic), vulnerable plaques all demonstrated higher RWS_{max} values than stable plaques (**Supplementary Table 4, Supplementary Table 5**). RWS_{max} maintained a high diagnostic performance (AUC=0.74–0.80), compared with DS% (AUC=0.55–0.71) and lesion length (AUC=0.60–0.70) (**Supplementary Table 3, Supplementary Figure 8**).

We performed logistic regression analyses to identify independent indicators of plaque vulnerability. The incidence of vulnerable plaque increased ~1.5 times for every 1% increase in RWS_{max}, in both plaque- and patient-level univariable analyses. Multivariable analysis showed RWS_{max} as a marker for plaque vulnerability at plaque level (adjusted odds ratio [OR] 1.45) – adjusting for DS% and lesion length – and at patient level (adjusted OR 1.48) – adjusting for age, sex, DS%, and lesion length (**Table 1**).

Plaque biomechanics can be assessed through elastograms derived from intravascular ultrasound measurements⁴. In our study, local radial strain was assessed with routine angiography by characterising the lumen diameter variation caused by

A summary of carotid RWS analysis, main findings and benefits of RWS.



- Benefits**
- No extra radiation or contrast agent exposure
 - Real time in catheter laboratory
 - Able to provide biomechanical information about plaques
 - Potential to optimise treatment

Shiteng Suo *et al.* • *EuroIntervention* 2025;21:e240-e243 • DOI: 10.4244/EIJ-D-24-00734

RWS_{max} allowed differentiation between vulnerable and stable plaques, as assessed by MRI, outperforming both DS% and lesion length in the evaluation. Angiography-derived RWS analysis provides a potential real-time and in-procedure method for evaluating plaque mechanics with no need for additional radiation or contrast agent exposure, thereby facilitating optimised procedures. Further longitudinal studies with predefined endpoints are needed to substantiate and validate these findings. AUC: area under the curve; DSA: digital subtraction angiography; DS%: percentage diameter stenosis; MRI: magnetic resonance imaging; RWS: radial wall strain; RWS_{max}: maximum RWS

Table 1. Unadjusted and adjusted associations between DSA parameters and carotid plaque vulnerability.

Independent variable	Univariable analysis		Multivariable analysis [†]	
	OR	p-value	OR	p-value
Per-plaque analysis*				
RWS _{max}	1.53 (1.28-1.83)	<0.001	1.45 (1.18-1.77)	<0.001
DS%	1.04 (1.02-1.07)	0.001	1.01 (0.98-1.04)	0.66
Lesion length	1.11 (1.04-1.19)	0.003	1.05 (0.98-1.13)	0.15
Per-patient analysis				
RWS _{max}	1.52 (1.25-1.85)	<0.001	1.48 (1.17-1.85)	<0.001
DS%	1.04 (1.01-1.07)	0.003	1.01 (0.98-1.04)	0.60
Lesion length	1.09 (1.01-1.17)	0.035	1.04 (0.96-1.13)	0.34
Age	1.02 (0.96-1.08)	0.58	1.00 (0.93-1.07)	0.98
Sex	0.57 (0.15-2.17)	0.41	0.44 (0.11-1.79)	0.25

Data in parentheses are 95% confidence intervals. *Adjusted for within-patient clustering by using mixed-effects logistic regression models. [†]The plaque-level multivariable model was adjusted by DS% and lesion length, and the patient-level model was adjusted by age, sex, DS% and lesion length. DS%: percentage diameter stenosis; OR: odds ratio; RWS_{max}: maximum radial wall strain

pulsatile arterial pressure³. We found that angiography-based RWS_{max} increased in vulnerable plaques and could serve as an independent factor of plaque vulnerability. These findings were consistent with previous simulation-based or histology-based studies^{5,6}, which demonstrated that atherosclerotic plaques predominantly comprised of soft tissues that destabilise the plaque integrity exhibited elevated strain values when subjected to mechanical forces. Extended exposure to high strain/stress on the lumen surface can precipitate endothelial dysfunction and diminish the strength of the lumen surface over time. Regions of high strain within plaques are reported to be colocalised preferentially to the plaque rupture site and are predictive of adverse events⁷.

The proposed method is simple, using just one angiographic view from routine DSA exams, which avoids extra radiation and contrast agent exposure. It offers interventionalists a potential real-time tool in the catheter laboratory to assess the mechanical properties of carotid plaques, aiding optimised procedures (**Central illustration**). Incorporating RWS into lesion-level risk assessment may facilitate the appropriate selection of embolic protection devices and stent types. It could also potentially serve as an alternative to judge plaque vulnerability when carotid MRI – often not routinely available – is absent. Furthermore, RWS may also have the capability to provide additional prognostic information beyond anatomical and functional assessments.

However, it is worth noting that the assessment of plaque vulnerability in this study, based on carotid MRI, does not always predict future rupture or adverse events. The prognostic value of RWS_{max} in carotid plaques still needs to be explored. The MRI features we used as a reference were not the only known non-invasive markers for increased neurological symptoms risk. Some other features, such as inflammation and neovascularisation, were not analysed. Additionally, different angiographic views, or even minor differences in the same view acquired at different timepoints or catheter laboratories, may affect the RWS results and require further research.

Other main limitations of this study included its retrospective design and suboptimal DSA frame rate, which have been fully discussed in **Supplementary Appendix 3**.

Angiography-based strain analysis proved feasible in carotid stenosis. RWS_{max} was correlated with vulnerable features and could identify high-risk plaques effectively regardless of stenosis severity or symptomatic status. Further validation and longitudinal studies are required to ascertain its clinical value in predicting events and guiding interventions.

Authors' affiliations

1. Department of Radiology, Renji Hospital, School of Medicine, and School of Biomedical Engineering, Shanghai Jiao Tong University, Shanghai, China; 2. Department of Radiology, Renji Hospital, School of Medicine, Shanghai Jiao Tong University, Shanghai, China; 3. Biomedical Instrument Institute, School of Biomedical Engineering, Shanghai Jiao Tong University, Shanghai, China; 4. Department of Cardiology, Huadong Hospital affiliated to Fudan University, Shanghai, China; 5. Department of Vascular Surgery, Zhongshan Hospital, Fudan University, Shanghai, China

Funding

This study was supported by the Leading Talent Program of Shanghai Municipal Health Commission (2022LJ023), Science and Technology Commission of Shanghai Municipality Explorer Project (22TS1400600), National Natural Science Foundation of China (82271942), and Renji Hospital (RJKY23-004, IIT-2024-0068).

Conflict of interest statement

S. Tu is a cofounder of, has received research grants from, and been a consultant for Pulse Medical. The other authors have no conflicts of interest to declare relevant to the contents of this paper.

References

- Kamtchum-Tatuene J, Noubiap JJ, Wilman AH, Saqqur M, Shuaib A, Jickling GC. Prevalence of High-risk Plaques and Risk of Stroke in Patients With Asymptomatic Carotid Stenosis: A Meta-analysis. *JAMA Neurol.* 2020;77:1524-35.
- Finet G, Ohayon J, Rioufol G. Biomechanical interaction between cap thickness, lipid core composition and blood pressure in vulnerable

coronary plaque: impact on stability or instability. *Coron Artery Dis.* 2004;15:13-20.

3. Hong H, Li C, Gutiérrez-Chico JL, Wang Z, Huang J, Chu M, Kubo T, Chen L, Wijns W, Tu S. Radial wall strain: a novel angiographic measure of plaque composition and vulnerability. *EuroIntervention.* 2022;18:1001-10.
4. Balocco S, Gatta C, Alberti M, Carrillo X, Rigla J, Radeva P. Relation between plaque type, plaque thickness, blood shear stress, and plaque stress in coronary arteries assessed by X-ray angiography and intravascular ultrasound. *Med Phys.* 2012;39:7430-45.
5. Wu X, von Birgelen C, Li Z, Zhang S, Huang J, Liang F, Li Y, Wijns W, Tu S. Assessment of superficial coronary vessel wall deformation and stress: validation of in silico models and human coronary arteries in vivo. *Int J Cardiovasc Imaging.* 2018;34:849-61.
6. Hansen HH, de Borst GJ, Bots ML, Moll FL, Pasterkamp G, de Korte CL. Validation of Noninvasive In Vivo Compound Ultrasound Strain Imaging Using Histologic Plaque Vulnerability Features. *Stroke.* 2016;47:2770-5.
7. Li C, Wang Z, Yang H, Hong H, Li C, Xu R, Wu Y, Zhang F, Qian J, Chen L, Tu S, Ge J. The Association Between Angiographically Derived Radial Wall Strain and the Risk of Acute Myocardial Infarction. *JACC Cardiovasc Interv.* 2023;16:1039-49.

Supplementary data

Supplementary Appendix 1. Methods.

Supplementary Appendix 2. Additional results.

Supplementary Appendix 3. Limitations.

Supplementary Table 1. MRI protocol.

Supplementary Table 2. Patient and plaque characteristics.

Supplementary Table 3. Diagnostic performance of different parameters for discriminating vulnerable from stable carotid plaques.

Supplementary Table 4. Imaging characteristics of stable and vulnerable carotid plaques according to stenosis severity.

Supplementary Table 5. Imaging characteristics of stable and vulnerable carotid plaques according to symptomatic status.

Supplementary Figure 1. Flowchart of subject recruitment.

Supplementary Figure 2. MRI features of carotid plaques.

Supplementary Figure 3. Histograms showing distributions of RWS_{max} , absolute lumen diameter change, and pixel number change of all analysed plaques.

Supplementary Figure 4. Bland-Altman plots with 95% limits of agreement.

Supplementary Figure 5. Relationship between RWS_{max} and morphological features of plaque.

Supplementary Figure 6. Relationship between RWS_{max} and plaque composition.

Supplementary Figure 7. Representative cases.

Supplementary Figure 8. Receiver operating characteristic curve analysis.

The supplementary data are published online at:

<https://eurointervention.pcronline.com/>

doi/10.4244/EIJ-D-24-00734



Supplementary data

Supplementary Appendix 1. Methods.

Study Population - The institutional ethics committee approved this retrospective study and waived the need for written informed consent. One author (S. Tu) is a consultant of Pulse Medical; however, the nonconsultant authors had control of the data and information submitted for publication. We searched the institutional database for consecutive patients with internal carotid artery (ICA) stenosis who underwent both carotid MRI and DSA examinations within one week between July 2019 and December 2021. Exclusion criteria included (1) ICA occlusion; (2) previous treatment history of endarterectomy, carotid artery stenting or neck radiation; (3) nonatherosclerotic vascular diseases, such as artery dissection or vasculitis; (4) incomplete MRI data or poor MRI image quality due to severe artefacts; (5) insufficient DSA image quality due to excessive overlap and foreshortening of the interrogated segment, severely blurred vessel margins, or incomplete contrast filling during one cardiac cycle (**Supplementary Figure 1**). Patients were defined as symptomatic if they had recently experienced ischemic stroke or transient ischemic attack (TIA) in the territory of the ipsilateral ICA stenosis without any other explanation for their stroke or TIA.

Carotid DSA - All intra-arterial DSA examinations were performed by experienced neuro-interventionalists with >10 years' experience on a digital angiography unit (Innova 4100, GE Healthcare, Milwaukee, WI or AXIOM Artis, Siemens Healthineers, Forchheim, Germany). Carotid angiography was performed in both anterior-posterior and lateral projections, as well as in extra projections if needed to better visualize the stenosis. A contrast agent (Iopamiro, Bracco Sine Pharmaceutical, Shanghai, China) with 370 mg iodine/ml was injected at a flow of 5 ml/s. Angiographic images were obtained at a rate of 6 frames/s, with a resolution of 0.10-0.24 mm per pixel size.

Carotid MRI - All subjects underwent carotid MRI on a 3.0T scanner (Ingenia, Philips Healthcare, Best, The Netherlands or Prisma, Siemens Healthineers, Erlangen, Germany). Carotid MRI protocol included three-dimensional (3D) time-of-flight (TOF) MRA, pre- and post-contrast T1-weighted volumetric isotropic turbo spin-echo acquisition (T1-VISTA) or 3D motion-sensitized driven equilibrium prepared rapid gradient echo (3D-MERGE) on the Ingenia scanner or T1-weighted sampling perfection with application-optimized contrast using different flip angle evolutions (T1-SPACE) sequence on the Prisma scanner. Post-contrast T1-VISTA, 3D-MERGE or T1-SPACE images were acquired 5 min after intravenous injection of gadolinium contrast agent (Magnevist, Bayer Schering Pharma AG, Berlin, Germany) with a dose of 0.1 mmol/kg and at a rate of 1.5 ml/s. **Supplementary Table 1** details the MRI protocols.

RWS analysis - RWS analysis was performed at an independent academic core laboratory (CardHemo, Shanghai Jiao Tong University) by one certified analyst (S. Suo) who was blinded to patients' clinical information and MRI data, using the AngioPlus Core software (version V3; Pulse Medical, Shanghai, China). A key frame with sharp lumen contours at the interrogated segment was selected from an optimal angiographic image projection with minimal overlap and foreshortening. After that, three other high-quality image frames were automatically determined by the software to represent different phases of the cardiac cycle along with the key frame (i.e., end-diastole, early-systole, end-systole, and mid-diastole). Lumen contours at the interrogated vessel were then outlined using an automatic

algorithm based on artificial intelligence and coregistered among all frames. RWS at each longitudinal position was computed as the difference between the maximum and the minimum lumen diameters within the cardiac cycle divided by the maximum diameter. RWS_{max} was defined as the highest RWS along the lesion segment. A representative example of RWS analysis is shown in **Central illustration**. Lesion length and percent diameter stenosis (DS%) according to NASCET criteria on DSA images were also recorded.

MRI image analysis - Two radiologists (J. Zhang and H. Zhao, with 5 and 11 years of experience in carotid MRI, respectively) who were blinded to clinical information, DSA images and RWS results independently analyzed the MRI data on the image viewing software (Vue PACS Livewire, Carestream, Rochester, NY). Any discordance between the two observers was resolved by consensus. Plaque components, such as calcification, lipid-rich necrotic core (LRNC), intraplaque haemorrhage (IPH), and fibrous cap rupture (FCR), were determined. The presence of calcification was defined as irregularly hypointense on all contrast-weighted images. LRNC was determined when there was an isointense region on TOF and pre-contrast T1-weighted images with no enhancement on post-contrast T1-weighted images. IPH was defined as a hyperintense area on TOF and pre-contrast T1-weighted images. FCR appears as an irregular luminal surface or a juxtaluminal hyperintense signal on TOF that connects with the hyperintense lumen. A large LRNC was defined as an LRNC that occupied $\geq 40\%$ of the vessel wall area on the transverse section. **Supplementary Figure 2** details the MRI features. Carotid plaque vulnerability determined by MRI was used as the reference standard. Current evidence suggests that certain carotid plaque component including large LRNC, IPH, or FCR was associated with a higher incidence of stroke, suggesting its potential as a marker for carotid plaque vulnerability. Therefore, in our study, the carotid plaque was deemed vulnerable if large LRNC, IPH, or FCR existed within the plaque. Besides, morphological features including maximum wall thickness (MWT) and normalized wall index (NWI; defined as wall area/total vessel area $\times 100\%$) were measured.

Statistical analysis - Data were tested for normality using the Shapiro-Wilk test. Continuous variables were expressed as mean \pm standard deviation (SD) if normally distributed, otherwise as median (interquartile range, IQR). Categorical variables were reported as number (percentage). Comparisons between groups were made using the Fisher's exact test or chi-square test for categorical variables while using the Student's t-test or Wilcoxon rank-sum test for continuous variables appropriately. The Spearman correlation analysis was applied to evaluate the association between RWS_{max} and plaque quantitative parameters as RWS_{max} was nonnormally distributed. The diagnostic performance of RWS_{max} for plaque vulnerability was evaluated using the area under the curve (AUC) by receiver operating characteristic (ROC) analysis, and the optimal cutoff value was determined by maximizing the Youden index. The DeLong method was used to compare the AUC values. Univariable and multivariable logistic regression analyses were performed to identify independent indicators of plaque vulnerability on a per-patient and per-plaque basis. The plaque-level analysis was adjusted for within-patient clustering by using mixed-effects logistic regression models. At the patient level, the index plaque was analyzed if patients had bilateral plaques. The index plaque was defined as the culprit plaque for symptomatic patients or the most stenotic plaque for asymptomatic patients. The multivariable model was adjusted by age, sex, and parameters with influence on a univariable level for patient-level analysis, and by lesion length and DS% for plaque-level analysis. Multicollinearity was assessed by the variance inflation factor, and variables with substantial multicollinearity, defined

as variance inflation factor greater than 2, were excluded from the multivariable analysis. To assess the intra- and interobserver agreement for RWS_{max} measurement, 40 randomly chosen datasets were analyzed by the same analyst one month later and by a second analyst. Intra- and interobserver agreement of RWS_{max} measurement was assessed with the Bland-Altman method and intraclass correlation coefficient (ICC) with a two-way mixed-effects model for absolute agreement. A two-sided $P < .05$ was considered to be statistically significant. Statistical analyses were performed using SPSS 22.0 (IBM Corporation, Armonk, NY), MedCalc v20.305 (MedCalc software, Ostend, Belgium) and STATA 18.0 (StataCorp, College Station, TX).

Supplementary Appendix 2. Additional results.

Reproducibility of RWS_{max} measurement - Bland-Altman plots with 95% limits of agreement for intra- and interobserver reproducibility are shown in **Supplementary Figure 4**. There was no proportional or fixed bias; the mean differences for intra- and interobserver reproducibility were 0.2% (95% CI: -4.7%, 5.0%) and 0.1% (95% CI: -4.9%, 5.1%), respectively. Intra- and interobserver agreement for RWS_{max} measurement was excellent with ICC values of 0.91 (95% CI: 0.83, 0.95) and 0.87 (95% CI: 0.77, 0.93), respectively.

Analysis time - RWS analysis was performed on a computer running a 64-bit Windows 10 operating system with AMD Ryzen 7 3750H processor, 16 GB of RAM, and 6 GB of GPU memory (NVIDIA GeForce RTX 2060). The average analysis time for each lesion was 59 ± 30 seconds.

Supplementary Appendix 3. Limitations.

Our study had limitations. First, the major limitation of this study was its retrospective design without external validation in a single center. Thus, it can only be classified as a proof-of-concept study, and the diagnostic value of RWS_{max} must be confirmed in prospective controlled studies. Besides, the retrospective nature of this study may have introduced inherent selection bias, with all patients having undergone both DSA and MRI examinations of carotid stenosis. In addition, a large proportion of patients and plaques had to be excluded because of previous treatment history, inappropriate lesion type and inadequate image sequences or quality. Of note, 4 frames were required for RWS analysis, therefore, only plaques having 4 frames with complete contrast filling during one cardiac cycle and sharp lumen edges could be included. Second, only MRI features of IPH, large LRNC and FCR were considered for plaque vulnerability. These MRI features were not the only known, non-invasive markers for increased neurologic symptom risk. Some other features, such as plaque inflammation and intraplaque neovascularization, were not analyzed. However, evidence on the association between inflammation and neovascularization and stroke is still inconclusive. Third, the interobserver agreement of MRI features was not evaluated in the study, although previous studies have demonstrated good interobserver reproducibility of morphological measurements and compositions of carotid plaques. Fourth, carotid DSA was acquired at 6 frames/s, which may be not optimal for strain analysis. Future validation studies using DSA acquired at higher frame rates are warranted.

Fifth, the prognostic value of RWS_{max} was not investigated. Prospective studies can be designed for this technique during carotid angioplasty and stent placement, in which the goal will be immediate assessment of carotid plaque (morphology plus mechanics), and investigate if a combined evaluation will aid in strategy optimization, distal embolization risk evaluation and prevention.

It's worth noting that the assessment of plaque vulnerability in this study was based on magnetic resonance component analysis, and these vulnerable plaques don't always lead to future rupture or adverse events. Most plaques initially classified as vulnerable or high-risk tend to remain stable over time, with only a very small proportion actually becoming unstable and causing adverse events. Previous studies on coronary artery disease have explored and established the association between plaque biomechanical indices and the risk of plaque rupture, highlighting the importance of biomechanics in assessing the vulnerability of atherosclerotic plaques. A recent study has demonstrated the added value of RWS in predicting target vessel failure. In future studies, it will be crucial to confirm that RWS_{max} , as a measure of carotid plaque vulnerability, actually correlates with an increased risk of carotid plaque rupture and cerebrovascular events.

In addition, there are other invasive imaging techniques capable of assessing the morphology and composition of plaques to determine their vulnerability, such as grayscale intravascular ultrasound (IVUS), virtual histology IVUS (VH-IVUS), near-infrared spectroscopy (NIRS) and optical coherence tomography (OCT). The insights offered by these imaging techniques contribute to evaluating the risk associated with plaques. For instance, high lipid core plaque assessed by NIRS was reported to be associated with cerebral embolism after carotid artery stenting. Quantitative VH-IVUS algorithm enables quantitative in vivo evaluation of the atherosclerotic plaque components and could be predictive of atherosclerotic clinical events. Our previous study in coronary arteries demonstrated a significant correlation between angiography-derived RWS and the composition of plaques, as well as established OCT indicators of plaque vulnerability, in subjects presenting with moderate coronary stenosis. However, these invasive imaging modalities are not routinely employed in the management of carotid artery plaques, as they introduce additional procedural complexities and financial burden on patients. In contrast, angiography-derived RWS analysis relies on standard DSA and offers supplementary plaque mechanical information beyond morphological assessment.

Supplementary Table 1. MRI protocol.

Parameter	Philips Ingenia		Siemens Prisma	
	3D TOF	T1-VISTA/3D-MERGE	3D TOF	T1-SPACE
TR (ms)	20	800/10.4	22	700
TE (ms)	4.9	19/4.8	3.7	13
Flip angle (°)	20	90/6	18	120
ETL	1	25/35	1	54
FOV (mm ²)	160×160	250×250/250×160	200×176	200×200
In-plane resolution (mm ²)	0.6×0.6	0.6×0.6/0.8×0.8	0.6×0.8	0.5×0.5
Slice thickness (mm)	1	0.6/0.8	0.7	0.5
Scan time	4:58	6:02/3:23	6:53	8:07

TOF= time-of-flight; T1-VISTA=T1-weighted volumetric isotropic turbo spin-echo acquisition; 3D-MERGE=3D motion-sensitized driven equilibrium prepared rapid gradient echo; T1-SPACE= T1-weighted sampling perfection with application-optimized contrast using different flip angle evolutions; TR=repeat time; TE=echo time; ETL=echo train length; FOV=field of view.

Supplementary Table 2. Patient and plaque characteristics.

Characteristic	All	With stable plaques	With vulnerable plaques	<i>P</i> value
Patient	<i>n</i> = 110	<i>n</i> = 30	<i>n</i> = 80	
Age (y)	67.7±7.2	67.1±7.8	67.9±7.0	.59
Sex (male)	94 (85.5)	27 (90.0)	67 (83.8)	.60
BMI (kg/m ²)	23.0 (21.7-25.0)	22.4 (20.7-24.9)	23.3 (21.9-25.1)	.14
Systolic BP (mmHg)	139.2±16.9	138.6±15.8	139.4±17.3	.83
Diastolic BP (mmHg)	78.2±11.2	79.8±9.5	77.7±11.7	.36
Vascular risk factors				
Hypertension	90 (81.8)	28 (93.3)	62 (77.5)	.10
Diabetes mellitus	42 (38.2)	10 (33.3)	32 (40.0)	.52
Hyperlipidemia	43 (39.1)	11 (36.7)	32 (40.0)	.75
Smoking	45 (40.9)	11 (36.7)	34 (42.5)	.58
Coronary artery disease	16 (14.5)	4 (13.3)	12 (15.0)	1.00
Ischemic stroke or TIA	79 (71.8)	21 (70.0)	58 (72.5)	.78
Laboratory parameters				
Total cholesterol (mmol/L)	3.4 (2.9-4.0)	3.4 (2.9-4.0)	3.4 (2.9-4.0)	.97
Triglycerides (mmol/L)	1.1 (0.8-1.5)	1.0 (0.9-1.5)	1.2 (0.8-1.6)	.30
HDL cholesterol (mmol/L)	1.0 (0.9-1.2)	1.1 (0.9-1.4)	1.0 (0.9-1.2)	.58
LDL cholesterol (mmol/L)	1.7 (1.4-2.2)	1.6 (1.4-2.1)	1.8 (1.4-2.2)	.61
FBG (mmol/L)	5.3 (4.8-6.0)	5.3 (4.8-5.8)	5.3 (4.7-6.1)	.75
Hemoglobin A1c (%)	6.0 (5.5-6.9)	5.9 (5.5-6.9)	6.0 (5.5-6.9)	.60
Plaque	<i>n</i> = 135	<i>n</i> = 41	<i>n</i> = 94	
DSA characteristics				
DS% (%)	58.6 (47.2-71.7)	52.6 (37.8-61.1)	63.2 (49.4-77.0)	<.001
Lesion length (mm)	14.0 (9.7-18.5)	11.3 (7.3-15.4)	15.1 (11.3-19.6)	.002
RWS _{max} (%)	9.5 (7.5-12.3)	7.5 (5.6-8.9)	11.0 (8.4-13.5)	<.001
MRI characteristics				
IPH	54 (40.0%)	0	54 (57.4%)	/
Large LRNC	70 (51.9%)	0	70 (74.5%)	/
FCR	34 (25.2%)	0	34 (36.2%)	/
Calcification	119 (88.1%)	38 (92.7%)	81 (86.2%)	.39
MWT (mm)	4.0 (3.4-5.0)	3.6 (2.8-4.6)	4.2 (3.7-5.3)	<.001
NWI (%)	78.1 (67.4-87.7)	68.2 (56.8-77.7)	82.7 (73.6-89.9)	<.001

Data are mean±standard deviation, median (interquartile range) or number (%). BMI=body mass index; BP=blood pressure; FBG=fasting blood glucose; HDL=high-density-lipoprotein; ICA= internal carotid artery; LDL=low-density lipoprotein, TIA=transient ischemia attack. DS%=percent diameter stenosis; RWS_{max}=maximum radial wall strain; IPH=intraplaque haemorrhage; LRNC= lipid-rich necrotic core; FCR=fibrous cap rupture; MWT=maximum wall thickness; NWI=normalized wall index.

Supplementary Table 3. Diagnostic performance of different parameters for discriminating vulnerable from stable carotid plaques.

Group and Parameter	AUC	Cutoff value	Sensitivity (%)	Specificity (%)	PPV (%)	NPV (%)
All plaques (<i>n</i> =135)						
RWS _{max} (%)	0.80 (0.72, 0.87)	>8.5	74.5 (64.4, 82.9) [70/94]	75.6 (59.7, 87.6) [31/41]	87.5 (80.1, 92.4) [70/80]	56.4 (46.7, 65.5) [31/55]
DS% (%)	0.70 (0.62, 0.78)	>58.2	62.8 (52.2, 72.5) [59/94]	73.2 (57.1, 85.8) [30/41]	84.3 (76.0, 90.1) [59/70]	46.2 (38.3, 54.2) [30/65]
Lesion length (mm)	0.67 (0.58, 0.75)	>12.7	68.1 (57.7, 77.3) [64/94]	63.4 (46.9, 77.9) [26/41]	81.0 (73.6, 86.7) [64/79]	46.4 (37.3, 55.8) [26/56]
Plaques with stenosis of <50% (<i>n</i> =42)						
RWS _{max} (%)	0.80 (0.65, 0.91)	>8.5	56.5 (34.5, 76.8) [13/23]	100.0 (82.4, 100.0) [19/19]	100.0 [13/13]	65.5 (54.4, 75.2) [19/29]
DS% (%)	0.55 (0.39, 0.70)	>47.2	30.4 (13.2, 52.9) [7/23]	94.7 (74.0, 99.9) [18/19]	87.5 (48.5, 98.1) [7/8]	52.9 (45.7, 60.1) [18/34]
Lesion length (mm)	0.70 (0.54, 0.83)	>13.3	60.9 (38.5, 80.3) [14/23]	79.0 (54.4, 93.9) [15/19]	77.8 (58.0, 89.9) [14/18]	62.5 (48.8, 74.5) [15/24]
Plaques with stenosis of 50% to 99% (<i>n</i> =93)						
RWS _{max} (%)	0.77 (0.67, 0.85)	>10.6	62.0 (49.7, 73.2) [44/71]	86.4 (65.1, 97.1) [19/22]	93.6 (83.5, 97.7) [44/47]	41.3 (33.4, 49.7) [19/46]
DS% (%)	0.71 (0.61, 0.80)	>63.9	63.4 (51.1, 74.5) [45/71]	77.3 (54.6, 92.2) [17/22]	90.0 (80.3, 95.2) [45/50]	39.5 (30.9, 48.9) [17/43]
Lesion length (mm)	0.61 (0.51, 0.71)	>12.7	70.4 (58.4, 80.7) [50/71]	54.6 (32.2, 75.6) [12/22]	83.3 (75.5, 89.0) [50/60]	36.4 (25.3, 49.1) [12/33]
Symptomatic plaques (<i>n</i> =79)						
RWS _{max} (%)	0.80 (0.70, 0.88)	>8.5	82.8 (70.6, 91.4) [48/58]	71.4 (47.8, 88.7) [15/21]	88.9 (80.1, 94.1) [48/54]	60.0 (44.5, 73.7) [15/25]
DS% (%)	0.67 (0.56, 0.77)	>57.6	63.8 (50.1, 76.0) [37/58]	66.7 (43.0, 85.4) [14/21]	84.1 (73.7, 90.9) [37/44]	40.0 (29.7, 51.3) [14/35]
Lesion length (mm)	0.69 (0.57, 0.79)	>12.3	72.4 (59.1, 83.3) [42/58]	61.9 (38.4, 81.9) [13/21]	84.0 (74.8, 90.3) [42/50]	44.8 (32.2, 58.1) [13/29]
Asymptomatic plaques (<i>n</i> =40)						
RWS _{max} (%)	0.74 (0.58, 0.87)	>10.5	42.9 (24.5, 62.8) [12/28]	100.0 (73.5, 100.0) [12/12]	100.0 [12/12]	42.9 (35.2, 50.8) [12/28]
DS% (%)	0.71 (0.55, 0.85)	>63.3	46.4 (27.5, 66.1) [13/28]	100.0 (73.5, 100.0) [12/12]	100.0 [13/13]	44.4 (36.2, 53.0) [12/27]
Lesion length (mm)	0.60 (0.43, 0.75)	>10.6	64.3 (44.1, 81.4) [18/28]	58.3 (27.7, 84.8) [7/12]	78.3 (63.6, 88.1) [18/23]	41.2 (26.0, 58.2) [7/17]

Data in parentheses are 95% confidence intervals, and data in brackets are numerators and denominators used to calculate percentages. AUC=area under the receiver operating characteristic curve; PPV=positive predictive value; NPV=negative predictive value; DS%=percent diameter stenosis; RWS_{max}=maximum radial wall strain.

Supplementary Table 4. Imaging characteristics of stable and vulnerable carotid plaques according to stenosis severity.

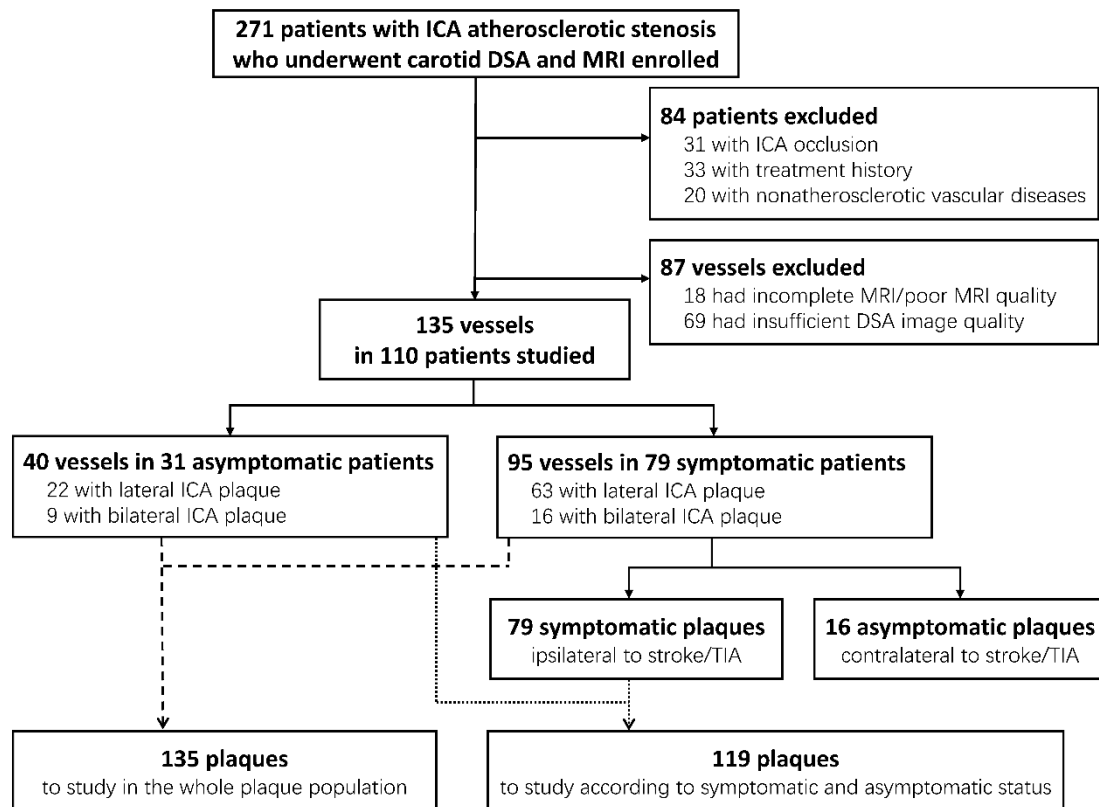
Characteristic	Stenosis of <50%			Stenosis of 50% to 99%		
	Stable	Vulnerable	<i>P</i> value	Stable	Vulnerable	<i>P</i> value
No. of plaques	19 (45.2%)	23 (54.8%)	/	22 (23.7%)	71 (76.3%)	/
DSA characteristics						
DS% (%)	37.6 (30.2-42.1)	38.7 (30.2-47.8)	.60	58.9 (53.8-64.4)	69.3 (59.3-81.1)	.003
Lesion length (mm)	8.8 (6.6-13.3)	15.5 (8.1-19.4)	.03	12.3 (9.4-16.5)	14.8 (12.0-19.9)	.12
RWS (%)	6.8 (5.2-7.5)	8.6 (6.9-10.0)	.001	8.5 (7.3-10.5)	11.6 (9.1-14.5)	<.001
MRI characteristics						
IPH	0	16 (69.6%)	/	0	38 (53.5%)	/
Large LRNC	0	13 (56.5%)	/	0	57 (80.3%)	/
FCR	0	8 (34.8%)	/	0	26 (36.6%)	/
Calcification	17 (89.5%)	21 (91.3%)	1.00	21 (95.5%)	60 (84.5%)	.28
MWT (mm)	3.1 (2.2-3.6)	4.0 (3.2-5.0)	.004	4.9 (3.9-5.5)	5.4 (4.3-6.1)	.13
NWI (%)	58.2 (52.2-68.0)	67.6 (60.4-76.1)	.04	81.5 (73.3-88.7)	91.0 (85.9-94.5)	<.001

Data are median (interquartile range) or number (%). DS%=percent diameter stenosis; RWS_{max}=maximum radial wall strain; IPH= intraplaque haemorrhage; LRNC= lipid-rich necrotic core; FCR=fibrous cap rupture; MWT=maximum wall thickness; NWI= normalized wall index.

Supplementary Table 5. Imaging characteristics of stable and vulnerable carotid plaques according to symptomatic status.

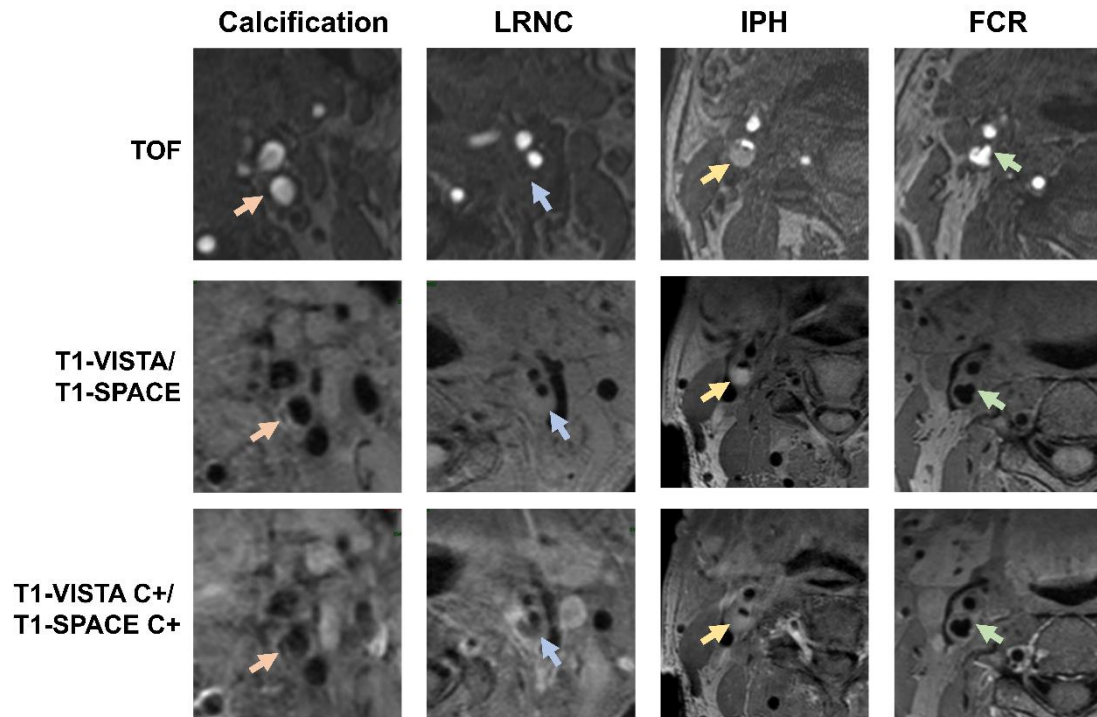
Characteristic	Symptomatic			Asymptomatic		
	Stable	Vulnerable	<i>P</i> value	Stable	Vulnerable	<i>P</i> value
No. of lesions	21 (26.6%)	58 (73.4%)	/	12 (30.0%)	28 (70.0%)	/
DSA characteristics						
DS (%)	53.7 (41.2-65.0)	64.9 (50.0-79.7)	.02	45.4 (37.7-61.9)	62.4 (50.7-76.4)	.03
Lesion length (mm)	12.0 (8.4-15.8)	16.2 (12.1-20.2)	.01	10.2 (7.2-16.4)	13.6 (9.1-19.2)	.32
RWS (%)	7.7 (6.1-10.4)	11.5 (9.2-14.3)	<.001	7.1 (5.6-8.4)	9.1 (7.4-13.0)	.02
MRI characteristics						
IPH	0	34 (58.6%)	/	0	15 (53.6%)	/
Large LRNC	0	46 (79.3%)	/	0	20 (71.4%)	/
FCR	0	23 (39.7%)	/	0	10 (35.7%)	/
Calcification	19 (90.5%)	48 (82.8%)	.62	11 (91.7%)	25 (89.3%)	1.00
MWT (mm)	3.6 (3.1-4.7)	4.2 (3.7-5.3)	.03	3.6 (2.2-4.4)	4.5 (3.8-5.4)	.008
NWI (%)	72.2 (60.3-79.6)	85.1 (74.1-90.6)	.001	65.1 (52.6-73.7)	81.9 (74.2-89.0)	<.001

Data are median (interquartile range) or number (%). DS%=percent diameter stenosis; RWS_{max}=maximum radial wall strain; IPH= intraplaque haemorrhage; LRNC= lipid-rich necrotic core; FCR=fibrous cap rupture; MWT=maximum wall thickness; NWI= normalized wall index.



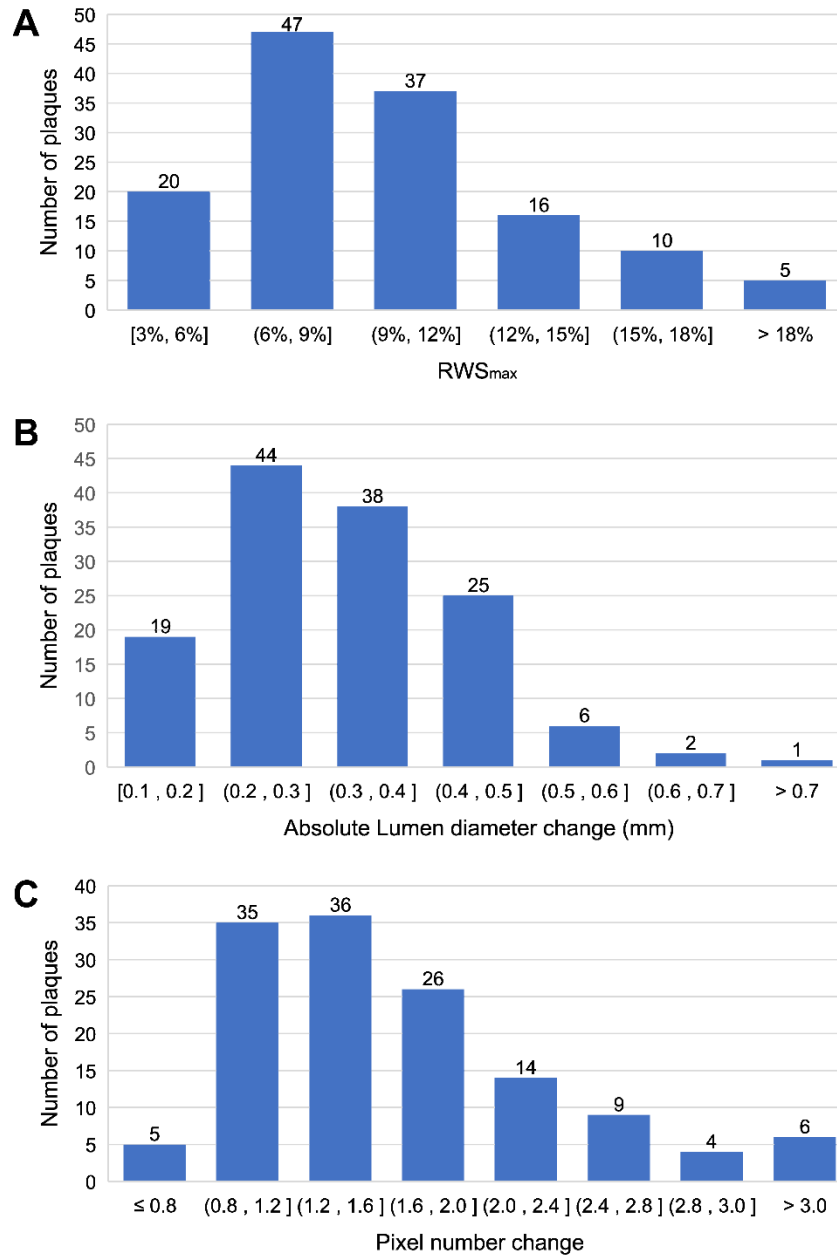
Supplementary Figure 1. Flowchart of subject recruitment.

ICA=internal carotid artery, TIA= transient ischemic attack.

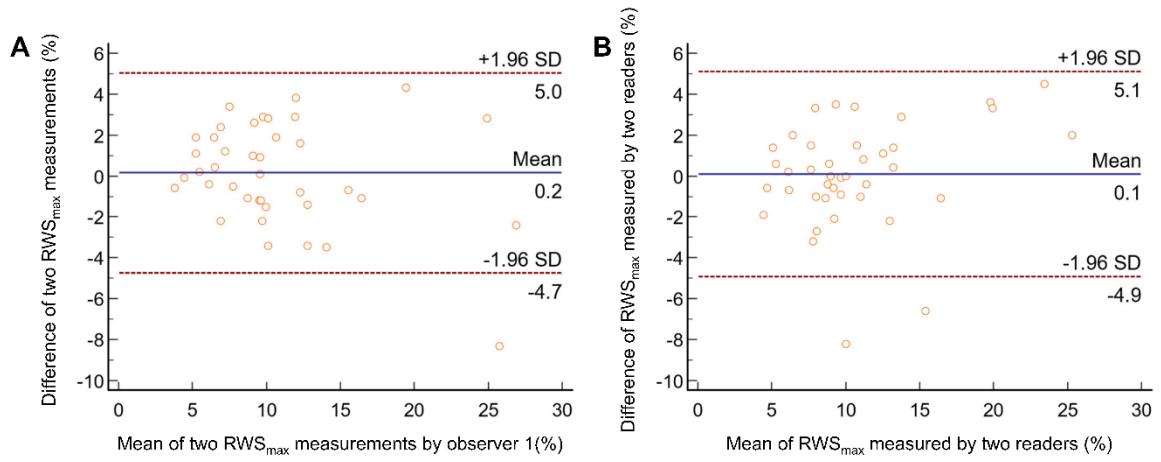


Supplementary Figure 2. MRI features of carotid plaques.

MRI sequences are shown in rows and features are shown in columns. In the first column, the hypointense signals (orange arrows) on all contrast-weighted images indicate the presence of calcification. In the second column, the blue arrows in all images show the lipid-rich necrotic core (LRNC), which appears isointense on time-of-flight (TOF) and pre-contrast T1-weighted images with no enhancement on post-contrast T1-weighted images. In the third column, the yellow arrows show hyperintense signals in the plaque on TOF and pre-contrast T1-weighted images that are compatible with intraplaque haemorrhage (IPH). In the fourth column, the fibrous cap rupture (FCR) characterized by irregular surface on all images and a hyperintense signal adjacent to the lumen on TOF are marked with green arrows. T1-VISTA=T1-weighted volumetric isotropic turbo spin-echo acquisition, T1-SPACE=T1-weighted sampling perfection with application-optimized contrast using different flip angle evolutions.

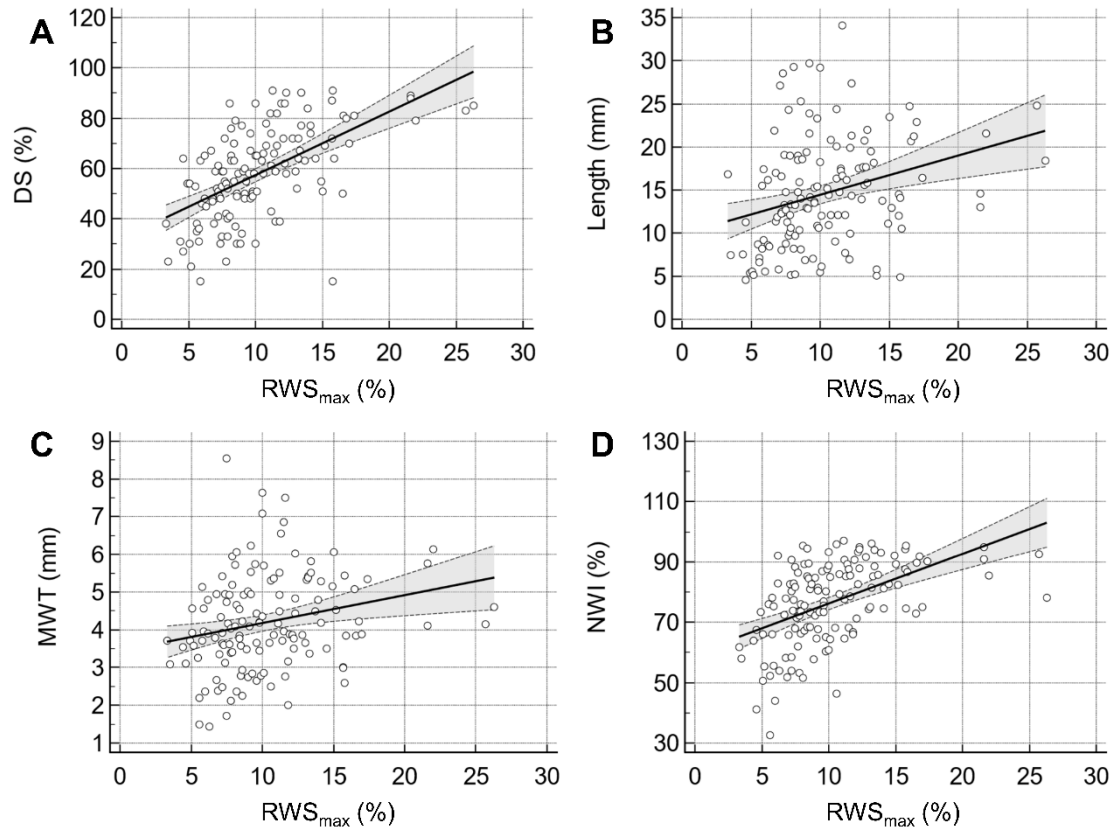


Supplementary Figure 3. Histograms showing distributions of RWS_{max}, absolute lumen diameter change, and pixel number change of all analysed plaques.



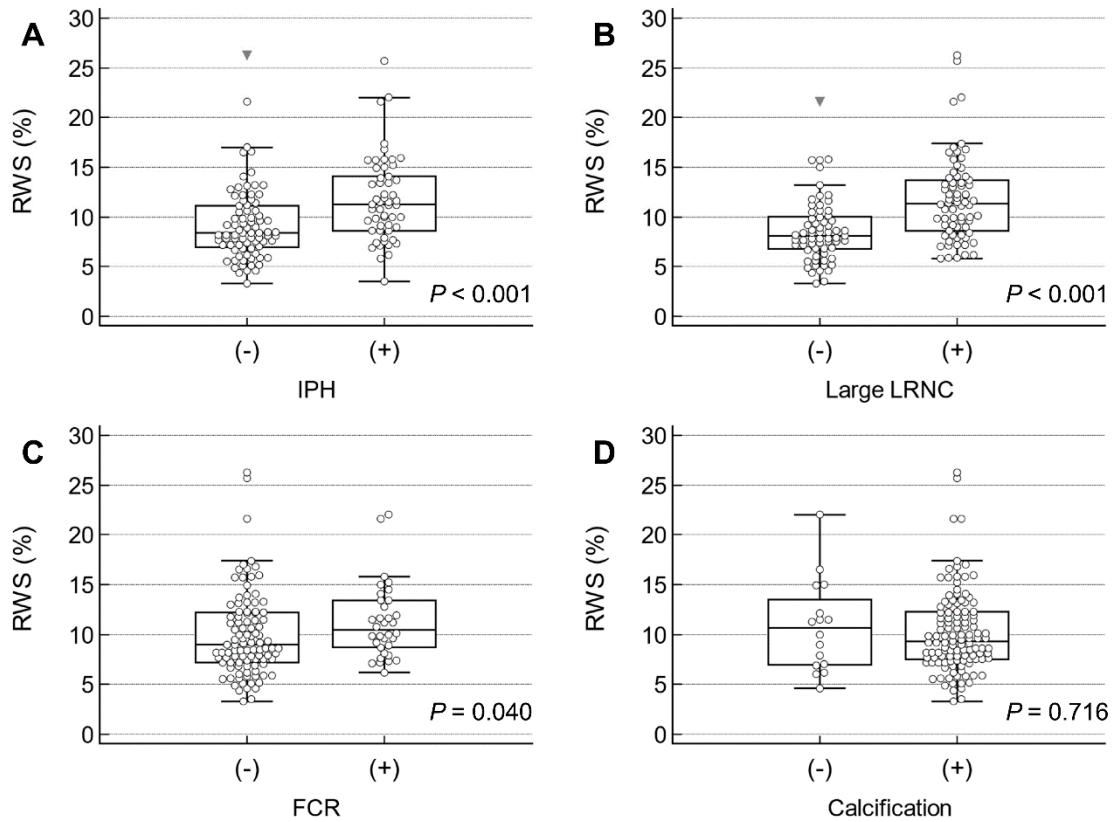
Supplementary Figure 4. Bland-Altman plots with 95% limits of agreement.

Good intraobserver (**A**) and interobserver (**B**) agreement for maximum radial wall strain (RWS_{max}) measurement are shown. SD=standard deviation.



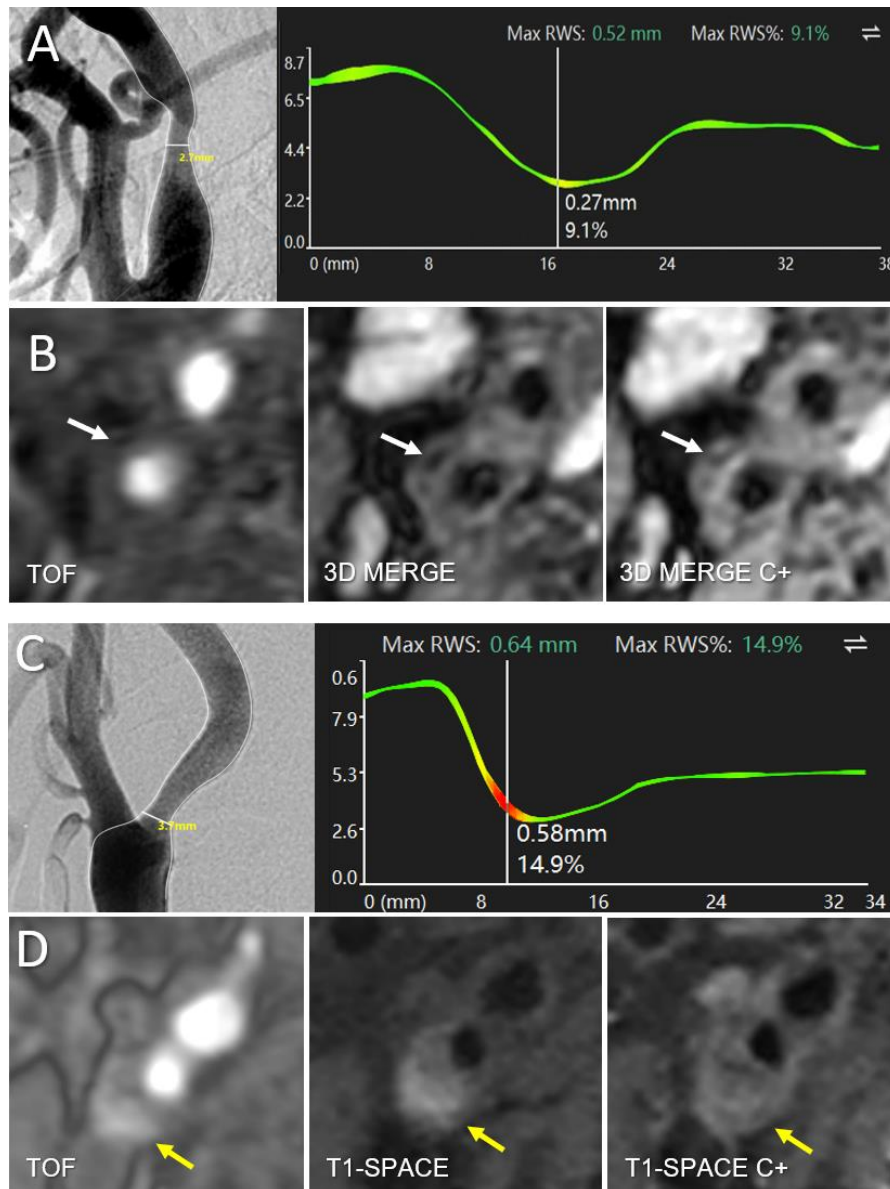
Supplementary Figure 5. Relationship between RWS_{max} and morphological features of plaques.

(A-D) Scatterplots show association of RWS_{max} with percent diameter stenosis (DS%), lesion length, maximum wall thickness (MWT), and normalized wall index (NWI), with Spearman ρ values of 0.60, 0.35, 0.30, and 0.55, respectively (all $P < .001$). The dashed lines indicate estimated 95% confidence intervals, and the solid line represents the fitting line.



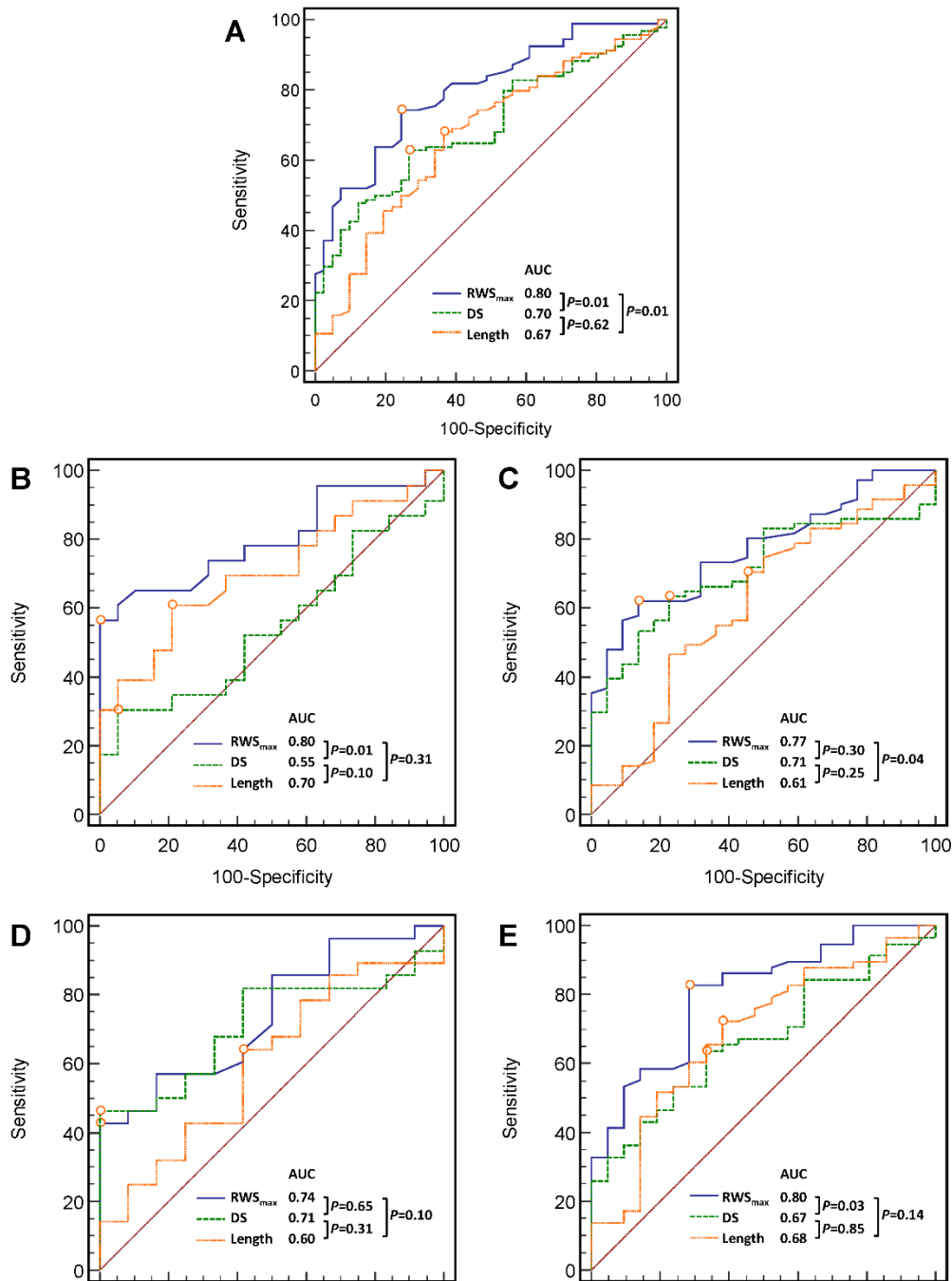
Supplementary Figure 6. Relationship between RWS_{max} and plaque composition.

(A-D) Box plots show RWS_{max} differences in carotid plaque groups with and without intraplaque haemorrhage (IPH), large lipid-rich necrotic core (LRNC), fibrous cap rupture (FCR), and calcification. The horizontal line in each box plot indicates the median, and the box corresponds to the IQR. The whiskers indicate minimum and maximum values. The data points represented by solid triangles are outliers.



Supplementary Figure 7. Representative cases.

(A, B) An adult patient diagnosed with ischemic stroke at admission. **(A)** Original DSA image showed 70% diameter stenosis of right cervical internal carotid artery segment. The position with a high strain pattern was found at the throat of the stenotic segment, with a maximum RWS (RWS_{max}) value of 9.1%. **(B)** Carotid MRI showed calcification with hypointensity on all contrast-weighted images (white arrows) and the plaque was classified as stable. **(C, D)** An adult patient diagnosed with ischemic stroke at admission. **(C)** The plaque of right cervical internal carotid artery segment shows a 55% diameter stenosis and a maximum radial wall strain (RWS_{max}) value of 14.9%. **(D)** Carotid MRI showed intraplaque haemorrhage with hyperintensity on time-of-flight (TOF) and pre-contrast T1-weighted sampling perfection with application-optimized contrast using different flip angle evolutions (T1-SPACE) images and no enhancement on post-contrast T1-SPACE image (yellow arrows). The plaque was classified as vulnerable. 3D MERGE=3D motion-sensitized driven equilibrium prepared rapid gradient echo.



Supplementary Figure 8. Receiver operating characteristic curve analysis.

Graphs show results of DSA imaging parameters including maximum radial wall strain (RWS_{max}), percent diameter stenosis (DS%), and lesion length for identifying carotid vulnerable plaques in different plaque subgroups. Analyses in (A) all plaques, (B, C) plaque subgroups with stenosis of <50% and 50% to 99%, and (D, E) symptomatic and asymptomatic subgroups all revealed the superior performance of RWS_{max} over DS% or lesion length. AUC=area under the ROC curve.